


Climatic and limnological changes at Lake Karakul (Tajikistan) during the last ~29 cal ka

Liv Heinecke  · Steffen Mischke · Karsten Adler · Anja Barth · Boris K. Biskaborn · Birgit Plessen · Ingmar Nitze · Gerhard Kuhn · Ilhomjon Rajabov · Ulrike Herzschuh

Received: 16 December 2016 / Accepted: 2 June 2017 / Published online: 16 June 2017
© Springer Science+Business Media B.V. 2017

Abstract We present results of analyses on a sediment core from Lake Karakul, located in the eastern Pamir Mountains, Tajikistan. The core spans the last ~29 cal ka. We investigated and assessed processes internal and external to the lake to infer changes in past moisture availability. Among the variables used to infer lake-external processes, high values of grain-size end-member (EM) 3 (wide grain-size distribution that reflects fluvial input) and high Sr/Rb and Zr/Rb ratios (coinciding with coarse grain sizes), are indicative of

moister conditions. High values in EM1, EM2 (peaks of small grain sizes that reflect long-distance dust transport or fine, glacially derived clastic input) and TiO₂ (terrigenous input) are thought to reflect greater influence of dry air masses, most likely of Westerly origin. High input of dust from distant sources, beginning before the Last Glacial Maximum (LGM) and continuing to the late glacial, reflects the influence of dry Westerlies, whereas peaks in fluvial input suggest increased moisture availability. The early to early-middle Holocene is characterised by coarse mean grain sizes, indicating constant, high fluvial input and moister conditions in the region. A steady

Electronic supplementary material The online version of this article (doi:[10.1007/s10933-017-9980-0](https://doi.org/10.1007/s10933-017-9980-0)) contains supplementary material, which is available to authorized users.

L. Heinecke (✉) · B. K. Biskaborn · I. Nitze · U. Herzschuh
Alfred Wegener Institute Helmholtz Centre for Polar and Marine Research, Research Unit Potsdam, Telegrafenberg A43, 14473 Potsdam, Germany
e-mail: Liv.Heinecke@awi.de

B. K. Biskaborn
e-mail: Boris.Biskaborn@awi.de

I. Nitze
e-mail: Ingmar.Nitze@awi.de

U. Herzschuh
e-mail: Ulrike.Herzschuh@awi.de

L. Heinecke · K. Adler · I. Nitze · U. Herzschuh
Institute of Earth and Environmental Science, University of Potsdam, Karl-Liebknecht-Str. 24-25, 14476 Potsdam-Golm, Germany
e-mail: Karsten_Adler@gmx.de

S. Mischke
Faculty of Earth Sciences, University of Iceland, Sturlugata 7, Askja, 101 Reykjavík, Iceland
e-mail: smi@hi.is

A. Barth
Institute of Geological Sciences, Free University of Berlin, Malteserstr. 74-100, 12249 Berlin, Germany
e-mail: barthanja77@gmail.com

B. Plessen
Helmholtz Centre Potsdam, GFZ German Research Centre for Geosciences, Sektion 5.2, Telegrafenberg C327, 14473 Potsdam, Germany
e-mail: Birgit.Plessen@gfz-potsdam.de

increase in terrigenous dust and a decrease in fluvial input from 6.6 cal ka BP onwards points to the Westerlies as the predominant atmospheric circulation through to present, and marks a return to drier and even arid conditions in the area. Proxies for productivity (TOC, TOC/TN, TOC_{Br}), redox potential (Fe/Mn) and changes in the endogenic carbonate precipitation (TIC, $\delta^{18}\text{O}_{\text{Carb}}$) indicate changes within the lake. Low productivity characterised the lake from the late Pleistocene until 6.6 cal ka BP, and increased rapidly afterwards. Lake level remained low until the LGM, but water depth increased to a maximum during the late glacial and remained high into the early Holocene. Subsequently, the water level decreased to its present stage. Today the lake system is mainly climatically controlled, but the depositional regime is also driven by internal limnogeological processes.

Keywords Arid Central Asia · Pamir Mountains · Lake sediments · XRF data · Grain-size end-member modelling · Geochemistry

Introduction

Interactions between the atmosphere and terrestrial environments have increasingly become the focus of research, especially since recent, human-mediated climate change has been acknowledged (Pielke et al. 1998; Williamson et al. 2008; Pachauri et al. 2014). In semi-arid and arid mountain regions, interactions among climate, glacial dynamics, water capacity of mountain lakes, and their influence on river-water discharge, need to be understood. The high mountain ranges of Central Asia are of particular interest within this context because of the complexity of regional

circulation mechanisms (Ramaswamy 1962; Aizen et al. 2001; Chen et al. 2010), the steep environmental gradients originating from pronounced relief, and their importance as freshwater sources for people who live in the region. Therefore, it is necessary to understand linkages between the atmosphere and terrestrial environments, and studies should not be based on modern observation alone, but rather should explore long-term processes, through paleoenvironmental inference.

Lake sediments can provide valuable paleoclimate information, but most paleolimnological studies in Central Asia have been carried out either on the Tibetan Plateau, in lower to mid-elevation mountain areas of western Central Asia, or in bordering basins (Van Campo and Gasse 1993; Shen et al. 2005; Zhao et al. 2009; Zhu et al. 2015). A literature search showed that studies from high mountain regions, like the Pamir, are rare (Huang et al. 2014; Lauterbach et al. 2014). Such studies focused on glacial activity (Zech et al. 2005; Abramowski et al. 2006; Liu et al. 2014), fluvial system development, and climatic-tectonic interactions (Fuchs et al. 2015). It remains unclear whether large and deep lakes in mountainous environments react rapidly to climate change or with some delay, or whether they are mainly internally driven and thus relatively unresponsive to climate change (Williamson et al. 2008).

Here we present a sediment record from Lake Karakul that dates back to ca. 29 cal ka BP. We used sediment geochemical data as proxies for conditions external to the lake and for exploring internal lake processes. Our first objective was to assess the reliability of these proxy variables. Second, we aimed to infer past climate changes, and by comparison with other records, we attempted to infer trends in past moisture availability. Third, we investigated whether internal lake processes were driven by or were independent from regional climate changes.

Study area

Lake Karakul (Tajik for ‘black lake’) is located at an altitude of 3915 m above sea level (asl) in the north-east of the autonomous Gorno-Badakhshan region of Tajikistan, in the eastern Pamir Mountains (Fig. 1), which are adjoined by the Hindukush and Karakorum ranges in the south and the Tian-Shan ranges in the north. The modern lake is brackish, with a pH of 9.2 (Mischke et al. 2010). The endorheic basin is supplied with freshwater that mainly originates from

G. Kuhn
Alfred Wegener Institute Helmholtz Centre for Polar and Marine Research, Am Alten Hafen 26,
27568 Bremerhaven, Germany
e-mail: Gerhard.Kuhn@awi.de

I. Rajabov
Pilot Program for Climate Resilience Secretariat,
Shevchenko Street 47, Dushanbe, Tajikistan

U. Herzsuh
Institute of Biochemistry and Biology, Karl-Liebknecht-
Str. 24-25, 14476 Potsdam-Golm, Germany

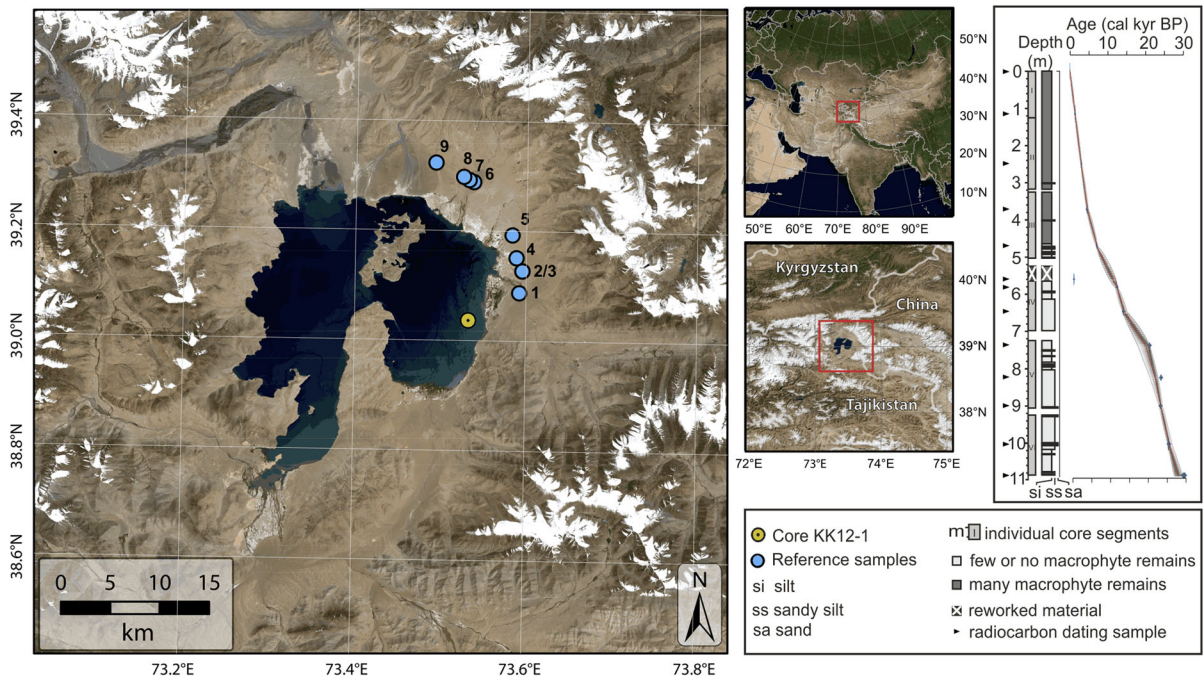


Fig. 1 Lake Karakul in the Pamir Mountains, Tajikistan, in arid Central Asia (Landsat-8 OLI image, 22 July 2014) and retrieved core KK12-1 including the age-depth model (for details, see ESM)

surrounding glaciers, snow fields and frozen ground, and enters the lake largely through two main streams in the north and south of the western sub-basin, and five smaller streams from the north, north-east and south in the eastern sub-basin (Mischke et al. 2010). Direct discharge from precipitation in the catchment is of minor importance (Ni et al. 2004) because precipitation is generally low, with an annual mean of only 82 mm, but characterised by high variability. The Westerlies, which are today the main moisture source (Böhner 2006), are blocked by the mountain ranges to the west. Air temperatures recorded by the meteorological station at Lake Karakul reveal a mean annual temperature of $-3.9\text{ }^{\circ}\text{C}$, mean $T_{\text{January}} -18.1\text{ }^{\circ}\text{C}$ and mean $T_{\text{July}} 8.5\text{ }^{\circ}\text{C}$ (measurement period 1934–2007, excluding 1995–2003). Low winter temperatures cause ice cover from November until May, with up to one metre of ice thickness. A maximum Secchi depth of 19 m was recorded during the open-water season (Ergashev 1979), whereas Secchi depths of 10.7–11.7 m were recorded in June 2008 (Mischke et al. 2010) and 3.4 m in August 2013. *Potamogeton pamiricus* and Characeae colonize the littoral zone (Hammer 1986). The terrestrial vegetation in the catchment is dominated by alpine steppe taxa such as

Stipa, *Oxytropis* and *Artemisia*. Direct human impact on the lake and its catchment is low.

Materials and methods

Fieldwork

Core KK12-1 (composite length 10.87 m) was collected during a field campaign in spring 2012 using UWITEC coring equipment (“Niederreiter 60”) at a water depth of 12 m. Coring was done from the ice cover on Lake Karakul, 1.8 km from the eastern shoreline (core site coordinates: 39.0176°N , 73.5327°E ; Fig. 1). Core KK12-1 was collected using a single ice hole. Small gaps occur between each 2-m core segment. Recovered sediment between 568 and 525 cm depth was disturbed during the previous core drive and is not in situ. Nine additional surface sediment samples were collected from different depositional settings (e.g. slackwater, pond, dry river channel, sand dune; Electronic Supplementary Material [ESM] Table S2) in the eastern to northern vicinity of the lake and used as reference material.

Laboratory analysis

Core sampling, lithology and age-depth model

The six sediment core segments were opened at the Alfred Wegener Institute in Potsdam. The “archive” halves were used for smear-slide analysis and non-destructive work such as initial core description and X-ray fluorescence (XRF) scanning. The “work” halves were subsampled for radiocarbon dating and sedimentological analyses (e.g. CNS (carbon, nitrogen, sulphur), total organic carbon (TOC), grain-size distribution and stable isotopes on carbonates).

The lithology from 1087 to 525 cm is characterised mainly by silt and sandy silt, with thin layers of sand (Fig. 1). Macrophyte remains are relatively rare or lacking in this section of the core. Sediments from 503 cm depth to the top of the core are characterised by silt with a few thin layers of sandy silt. Sediments above 465 cm depth contain very abundant macrophyte remains. The macrophyte remains are Potamogetonaceae leaves that are embedded horizontally in the sediments.

Fourteen samples, nine consisting of plant remains, four of bulk sediment and one of an in situ-collected living charophyte were dated at the Poznań Radiocarbon Laboratory, Poland (ESM Table S1). Radiocarbon ages were corrected for the ‘reservoir effect’ of Lake Karakul using the published value of 1.420 ka (Mischke et al. 2010) and the apparent age of the newly collected macro-algae. The lake reservoir effect calculation was based on the ^{14}C concentration of the atmosphere in the year of the sampling (2012). Thus, the post-bomb ^{14}C concentration of the atmosphere in 2012 was used for the calculation of the $F^{14}\text{C}$ (fraction modern) of 0.8914 (Reimer et al. 2004; Mischke et al. 2013). The obtained $F^{14}\text{C}$ value is equivalent to a lake reservoir effect of 1315 years. The average of the two determined lake reservoir effects, i.e. 1368 years, was applied to correct the radiocarbon age data from the core. No terrestrial macrofossils were found in the core, and we tentatively assume that the lake reservoir effect did not change markedly through time. The mean lake reservoir effect of 1368 years was used in the age-depth model (Fig. 1; ESM Fig. S1) created with the Bacon package (Blaauw and Christen 2011) in R (R Core Team 2012). Bacon parameter settings largely follow Blaauw and Christen (2011), but we set the mean

accumulation rate to 20 year cm^{-1} prior to the model run and 20 for the memory strength to account for bioturbation effects, originating from the dense macrophyte cover. The obtained age-depth models were fairly robust despite variations in the parameter settings.

Geochemistry

Smear slides were prepared and inspected approximately every 40 cm. Total carbon (TC), total nitrogen (TN), total sulphur (TS) and TOC were analysed for 97 samples taken at 10-cm intervals. The freeze-dried and finely ground samples for element analyses were weighed into tin capsules for CNS determinations and measured using an Elementar vario EL III (CNS) analyser. An Elementar vario MAX C was used to quantify TOC. TN values in the lower part of the core were occasionally at, or close to the detection limit at 0.1%, however the data were still used to calculate TOC/TN ratios. Total inorganic carbon (TIC) was calculated by subtracting TOC from TC values.

Stable isotope analyses on authigenic carbonates were conducted on 98 samples, which were bleached for 24 h with 2.5% NaOCl to remove organic matter and sieved with a 36- μm mesh to clean the samples of detrital components and shells. The remaining authigenic carbonate fraction was freeze-dried, ground for homogenization and loaded into Labco vials. Measurements of $\delta^{13}\text{C}_{\text{Carb}}$ and $\delta^{18}\text{O}_{\text{Carb}}$ were undertaken with a ThermoFinnigan Gasbench II linked to a DELTA^{plus}XL mass spectrometer and measured after digestion with 103% H_3PO_4 at 72 °C for 60 min at the German GeoForschungsZentrum (GFZ) in Potsdam. The stable isotope data are reported in per mil relative to VPDB and were calibrated using NBS19 with an analytic precision error of <0.08% for both $\delta^{13}\text{C}$ and $\delta^{18}\text{O}$ on reference material.

Grain-size analysis

Preparation of 97 samples for grain-size analysis included 24 h of treatment with CH_3COOH (10%) to remove carbonate, sieving with a 2-mm sieve to remove abundant plant remains in most parts of the core, and shaking the samples on a platform shaker, initially in a 0.3% H_2O_2 solution, with an addition of 10 ml of H_2O_2 (35%) every second day, for up to six weeks to remove the remaining organic matter. Grain-

size analysis was performed with a Coulter LS 200 Laser Diffraction Particle Analyser, which was equipped with a 1-mm sieve to protect the lens. At least two subsamples were measured for every sample.

XRF analysis

High-resolution non-destructive XRF measurements were performed at the Alfred Wegener Institute, Bremerhaven, with an Avaatech XRF Core Scanner. An additional 26 single samples were measured for calibration purposes (see the ESM for details).

Multivariate statistics

Different transport and deposition processes can be deciphered from grain-size distribution data using end-member modelling analyses (EMMA; Weltje 1997). The obtained grain-size data were analysed with the EMMAgeo package (Dietze and Dietze 2013) in R (R Core Team 2012). To achieve the best fit between modelled and measured data, we performed several model runs with different percentiles (P3/P97, P4/P96, P5/P95, P6/P94, P7.5/P92.5 and P10/P90; ESM Table S2). The minimum number of potential end-members was determined by the cumulative variance that explained 95% of the total variance of the original grain-size data, whereas the maximum number of potential end-members was determined by the mean coefficient of determination, which reflects the explained variance (mean r^2 ; Dietze et al. 2012). To avoid overfitting, we used a model with P3/P97 and four robust and one residual EM, representing the unexplained variance.

Several statistical analyses were applied to portray the main structure in the data set, such as the relationship among single variables, and between variables and samples. To gain better insight into the system we differentiated between external and internal lake variables. A detailed description of the proxies used is included in the first part of the discussion. Lake external parameters are in general characterised as parameters of an externally forced nature, such as grain-size distribution, which is assumed to reflect input to the lake of minerogenic proxies for detrital matter. On the other hand, lake internal parameters are those related to internal processes and mainly form within the lake. Principal component analyses (PCA) were applied after the data were square-root

transformed, centred and standardized in CANOCO version 5 (Ter Braak and Šmilauer 2012). A stratigraphically constrained incremental sum of squares analysis (CONISS) in Tilia version 1.7.16 was applied to the square-root transformed data to identify significant changes in the data and assign zones (Grimm 1987).

Results

Age-depth relationship in core KK12-1

A lake-reservoir effect of 1.368 ka was determined using dates on two in situ-collected living charophytes. Results of the lake reservoir-effect-corrected and calibrated samples (ESM Table S1) and the age-depth model (Fig. 1; ESM Fig. S1) show an age of ca. 29 cal ka BP at the base of core KK12-1. The mean sediment accumulation rate is 0.49 mm a⁻¹ and ranges from 0.15 mm a⁻¹ in the lower part of the core to 0.84 mm a⁻¹ at the top, which is, in addition to changes in sediment input, mainly a consequence of changes in the abundance of macrophyte remains in the core.

TIC, TOC, TOC/TN, $\delta^{18}\text{O}_{\text{Carb}}$ and $\delta^{13}\text{C}_{\text{Carb}}$

Core KK12-1 consists of a sequence of fine-grained, greyish sediment with a variable amount of plant remains. TIC ranges between 1.7 and 8.6% (median: 3.0%; Fig. 2b) and is generally characterised by high sample-to-sample variation. Lowest values occur between 982 and 692 cm (26.3 and 17 cal ka BP) and the highest values between 682 and 402 cm (16.5 and 5.3 cal ka BP). TOC ranges from 0.1 to 2% at 1082 and 452 cm (28.5 and 6.6 cal ka BP), followed by a sharp increase with values reaching 5.3% in the upper part of the core (median 1.6%).

TOC/TN ratios display low values. Results from below 692 cm (17 cal ka BP) are unreliable because TN was close to the detection limit. Highest values were determined between the two maxima at 332 and 172 cm (4.1 and 2.0 cal ka BP; Fig. 2b).

Values of $\delta^{13}\text{C}_{\text{Carb}}$ vary between 1.4 and 4.9‰ (median: 3.7‰). $\delta^{18}\text{O}_{\text{Carb}}$ displays values from -7.4 to -0.3‰ (median -3.1‰). Both stable isotope datasets show similar trends over the core, with high values from the core base to 1025 cm (28.6 to

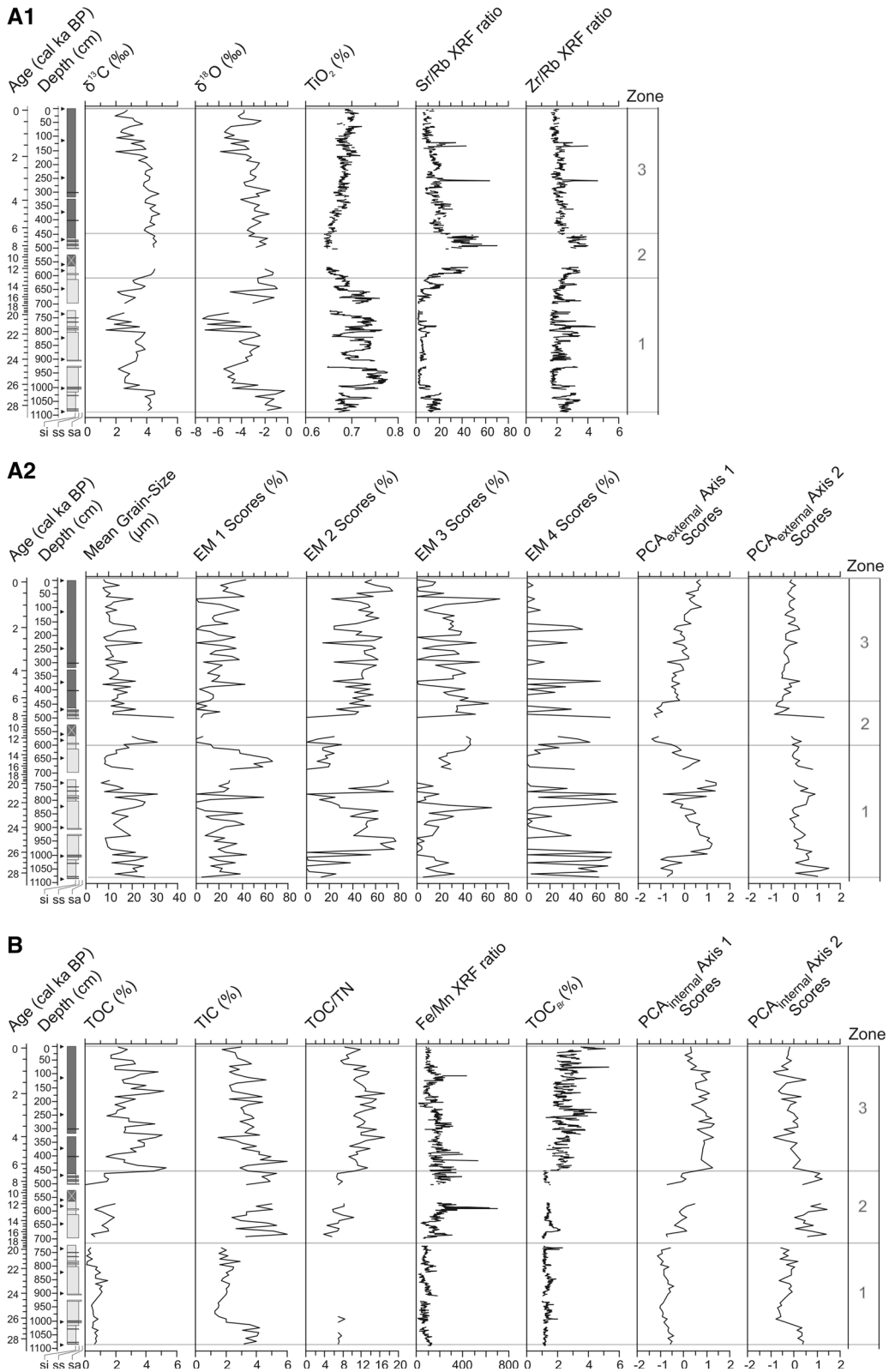


Fig. 2 Geochemical and sedimentological data for core KK12-1 including PCA Axis Scores. CONISS was used to identify zone boundaries. **a.1** and **a.2**—for lake external parameters, **b**—for lake internal parameters

26.5 cal ka BP), a rapid decrease and generally lower values until 652 cm (14.7 cal ka BP), a period of higher values until 292 cm (3.5 cal ka BP) and a decreasing trend to the core top (Fig. 2a.1).

Grain-size distribution and results of end-member modelling

Mean grain-size varies mainly between 7 and 31 μm (median 12 μm). A slight decreasing trend in mean grain-size and generally less variation were identified in the upper 500 cm (<8.1 cal ka BP). The final end-member model (P3/P97) results in four robust EMs and one residual EM (Fig. 3a). All four EMs show bimodal or polymodal grain-size frequency distribution curves, with the main peak at 2–4 μm for EM1, 10–20 μm for EM2, 20–50 μm for EM3 and 100–300 μm for EM4. EM1 accounts for 15.2% of the detrital sediments over the core, EM2 for 30.1%, EM3 for 18.5% and EM4 for 35.6%. EM1 and EM2 have relatively high abundances throughout the core, whereas EM3 and EM4 show larger fluctuations (Fig. 2a.2). The very fine-grained EM1 reaches its highest values, up to 67%, between 672 and 622 cm (15.8 and 13.6 cal ka BP). EM2 is most abundant from 982 to 942 cm (25.8 to 25.0 cal ka BP) with a maximum of 78%, and between 772 and 732 cm (21.0 to 19.5 cal ka BP), with a maximum of 76%. It is constantly recorded in medium to high proportions

(>25%) from 492 cm upward (8 cal ka BP to present). EM3 shows peaks of 61% at 832 cm (22.7 cal ka BP), 60% at 452 cm (6.6 cal ka BP) and 65% at 72 cm (0.8 cal ka BP). Peaks for EM4, with maxima up to 73, 79 and 72%, are recorded from the core base until 992 cm (28.6 to 26.2 cal ka BP), from 822 to 782 cm (22.4 to 21.2 cal ka BP) and at 502 cm (8.6 cal ka BP).

XRF data

XRF scanning analyses revealed values from 1.7 to 70.3 for Sr/Rb ratios (median 11.0), 1.4 to 4.6 for Zr/Rb ratios (median 2.1), and 17.3 to 703.1 for Fe/Mn ratios (median 114.3). Br has been reported to be an indicator for organic matter in lake sediments (Biskaborn et al. 2013). Because of the good correlation between TOC and XRF Br, we quantified TOC_{Br} from the peak area intensities of Br, to use it as a high-resolution proxy for the organic carbon content. TOC_{Br} ranges from 0.8 to 5.7% (median 1.51%), showing a rapid increase at 449 cm (6.6 cal ka BP) and high variability in the upper part of the core. The calibrated TiO₂ concentrations vary between 0.64 and 0.79% (median 0.69%). TiO₂ shows relatively large fluctuations, with an overall decrease from the base to the middle of the core, and lower but constantly increasing values towards the top. Peaks in Sr/Rb and Zr/Rb ratios are mainly correlated with high EM4 portions.

Ordination results of sediment parameters

The first two PCA axes of the lake-external parameters explain 62.9% of the variance (Fig. 4a). TiO₂, EM1

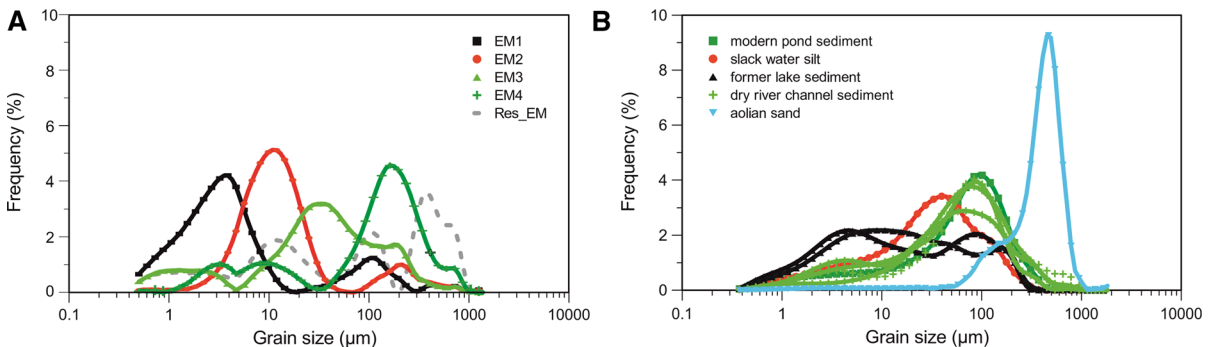


Fig. 3 End-member modelling for core KK12-1. **a**—Loading of grain-size-based end-member modelling of Lake Karakul, **b**—grain-size distribution of the nine reference samples in the vicinity of Lake Karakul

and EM2 plot on the positive end of the first axis. Opposite to EM1 and correlated with each other are the Zr/Rb ratio and the $\delta^{18}\text{O}_{\text{Carb}}$ values, which are also correlated with the $\delta^{13}\text{C}_{\text{Carb}}$ values, the Sr/Rb ratio and EM3 in the lower left of the PCA plot. EM4 and EMres plot in the upper left and are negatively correlated with EM2. The first two PCA axes of the lake-internal parameters explain 81.1% of the variance of the data. TOC, TOC_{Br} and the TOC/TN ratio plot in the lower right quadrant, whereas TIC and the Fe/Mn ratio plot in the upper right part of the PCA plot (Fig. 4b).

The stratigraphically constrained cluster analysis suggests a division of the core into three zones for the external parameters. External parameter zone 1 (core base to 613 cm; 28.6 to 13.3 cal ka BP) shows negative PCA axis 1 scores up to 1012 cm depth (26.5 cal ka BP) and mostly positive values above, whereas PCA axis 2 scores are almost exclusively positive (Fig. 2a.2). Zone 2 (602 to 452 cm; 13 to 6.6 cal ka BP) plots with a decreasing trend from positive to negative axis 1 scores and variable, mainly positive axis 2 scores. The external parameter zone 3 (442–0 cm; 6.6 cal ka BP to present) is characterised by increasing trends for axis 1 and slightly increasing axis 2 sample scores (Fig. 2a.2).

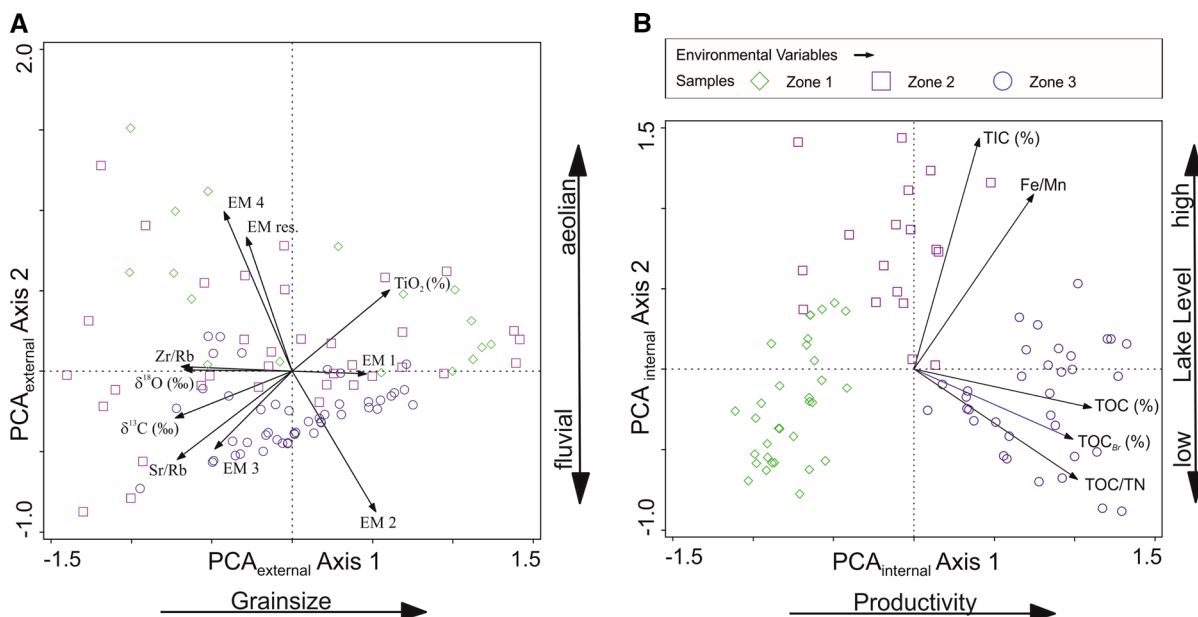


Fig. 4 Biplot for principal component analyses (PCA) of geochemical and sedimentological parameters for core KK12-1. **a**—for external parameters zone 1: 28.6–13.3 cal ka BP, zone

The stratigraphically constrained cluster analysis for the internal parameters also results in three zones. Samples from internal parameter zone 1 (core base to 713 cm; 28.6–19.2 cal ka BP) present negative PCA axis 1 and positive and negative PCA axis 2 scores. PCA axis 1 sample scores for the internal parameter zone 2 (712–462 cm, 17.5–6.9 cal ka BP) show an increasing trend with mainly negative values, whereas axis 2 scores are positive throughout zone 2, after rapidly increasing at the beginning of the zone (Fig. 2b). The internal parameter zone 3 (452–0 cm; 6.6 cal ka BP to present) shows slightly decreasing, still positive axis 1 scores and both positive and negative, but slightly decreasing axis 2 scores (Fig. 2b).

Discussion

Paleoenvironmental indicators from sediment variables

TOC concentrations reflect preserved organic matter content (Fig. 2b), i.e. the balance between allochthonous organic matter input, autochthonous organic matter production, and degradation (Meyers and

2: 13.3–6.6 cal ka BP, zone 3: 6.6 cal ka BP to present; **b**—for internal parameters zone 1: 28.6–18.4 cal ka BP, zone 2: 18.3–6.6 cal ka BP, zone 3: 6.6 cal ka BP to present

Lallier-Vergés 1999). The major part of TOC in core KK12-1 was probably formed in the lake, given the high abundance of aquatic plant remains. Sparse terrestrial vegetation and low precipitation in the modern catchment of Lake Karakul support the assumption that terrestrial organic matter did not contribute markedly to organic matter accumulation on the lake floor. Accordingly, no terrestrial macrofossil remains were found in the sediments of the core. Thus, considerable input of terrestrial organic matter, which was recorded in Ahung Co on the south-central Tibetan Plateau, did not occur in the drier setting of Lake Karakul (Morrill et al. 2006). We consider Br to be a complementary high-resolution proxy for organic matter content, consistent with previous studies of marine (Mayer et al. 1981; Ziegler et al. 2008) and lake sediments (Kalugin et al. 2007; Biskaborn et al. 2013). The TOC/TN ratios (Fig. 2b) likely reflect the source of sediment organic matter at the core site. Values between 4 and 10 indicate dominance of phytoplankton, whereas values ≥ 18 indicate a greater contribution from vascular plant sources (Meyers and Lallier-Vergés 1999). Thus, the TOC/TN ratios of core KK12-1 indicate a mix of sources, including lacustrine algae and submerged vascular plants. Combined interpretation of TOC concentrations and TOC/TN ratios may indicate bioproductivity variations in Lake Karakul.

TIC reflects the carbonate content (Fig. 2b), most likely originating from allochthonous input of detrital sediments from the catchment and/or as dust, and/or through precipitation from the water column (Cohen 2003). Visual inspection of smear slides indicated that the carbonate fraction comprises endogenic aragonite crystals, and shells and shell fragments of ostracods and aquatic gastropods. It cannot, however, be ruled out that detrital carbonate from the southern part of the catchment is transported to the lake during sporadic floods and that fine-grained carbonate particles of aeolian origin also accumulated in the lake basin (Strecker et al. 1995).

The strong correlation between $\delta^{13}\text{C}_{\text{Carb}}$ and $\delta^{18}\text{O}_{\text{Carb}}$ ($r = 0.82$), measured from the authigenic carbonate fraction, reflects the closed-basin setting of Lake Karakul (Talbot 1990). $\delta^{13}\text{C}_{\text{Carb}}$ values (Fig. 2a.1) are influenced by the productivity in the surface waters of the lake, where phytoplankton preferentially incorporate ^{12}C , which leaves the water column enriched in ^{13}C . $\delta^{13}\text{C}_{\text{Carb}}$ values are also

controlled by climate conditions, including precipitation and evaporation (Talbot 1990). Precipitation at Lake Karakul is, however, generally low and accordingly, glaciers and snowfields represent the main water sources. Therefore, we assume that $\delta^{18}\text{O}_{\text{Carb}}$ values mostly reflect evaporation/freshwater input ratios and temperature, rather than changes in the amount of precipitation. The long-term $\delta^{18}\text{O}$ signal is additionally affected by changes in the $\delta^{18}\text{O}$ signature of the water source (i.e. the ice-volume effect) and the large temperature change over a glacial-interglacial cycle.

End-member modelling of grain-size data was applied to decipher different transport and deposition processes of the inorganic non-carbonate sediment fraction (Weltje 1997). Taking into account the grain-size distribution in the sediments from core KK12-1 and of modern reference samples (Fig. 3b and Table S2), the end-member modelling results imply that the Lake Karakul core sediments reflect four different sediment populations (Fig. 2a.2). Individual end-members, however, do not necessarily represent a single process, but may result from different sources and transport mechanisms, and can be deposited in mixed composition in different sedimentary environments.

EM1, with its narrow peak in the fine-grained fraction, likely represents very fine aeolian dust that was transported over large distances in high-suspension clouds (Wu et al. 2006) and deposited from the atmosphere via precipitation (Vandenberghe et al. 2006; Dietze et al. 2012). Therefore, EM1 might be indicative of the influence of the Westerlies air stream. Furthermore, EM1 could also be regarded as very fine clastic input derived from glacial meltwater, so-called “glacial milk” (Wang et al. 2015), and point towards increased glacier melt.

EM2 shows a main peak in the fine-moderate silt fraction. Thus EM2 (and grain size) is also likely to reflect remote sources of wind-transported material (Tsoar and Pye 1987; Sun et al. 2002). Loess deposits are not common in the Pamir-Alay region above 3000 m asl, so EM2 most likely represents aeolian sediments transported over long distances (Vandenberghe 2013). The fine-grained sediments of EM2, however, may also include the suspension load of glacial outwash material or rock flour (Boulton 1978), which is unidentifiable through grain-size measurement and EMMA.

EM3 covers a wide grain-size range and its dominant grain size can also be found in the reference samples of the modern pond sediment, slack-water silt and dry-river-channel sediment (Fig. 3b and Table S2). The wide range and polymodal distribution are likely indicative of fluvial deposits (Walling and Moorehead 1989). Hence, its downcore distribution probably represents fluvial input to the lake. Accordingly, high portions of EM3 sediments in core KK12-1 are tentatively interpreted as proxies for moister conditions at the study site, although meltwaters from glacier tongues approaching the lake, and local aeolian sediments from alluvial fans and plains, may have also contributed to the accumulation of the relatively poorly sorted silts and fine sands of EM3 (Vandenbergh 2013).

EM4 shows similarities with the reference sample of well-sorted aeolian sand. Its coarse grain size indicates a local source area of hundreds of metres to a few kilometres distance. Although the source of this coarse grain-size fraction is possibly influenced by glacial activity, through formation of unconsolidated sediments by glacial erosion in the area, glaciers are probably not the main means of transport into the lake and to the core location. Because of the distance of the core location from the modern shoreline, and the paleo-shorelines above the lake, we favour transport by strong local winds, especially during winter and under snow-free conditions, which enabled saltation and creep of grains and transport onto the frozen lake surface (Tsoar and Pye 1987; Sun et al. 2002; Mischke et al. 2010).

Quantitative, single-sample XRF measurements over the core enabled the calibration of XRF-scanner data, which resulted in semi-quantitative data (Weltje and Tjallingii 2008; Biskaborn et al. 2013). We used Titanium (Ti) and its oxide (Fig. 2a.1) as a proxy for fine clastic input to the lake (Fey et al. 2009; Kylander et al. 2011). Sr/Rb and Zr/Rb were interpreted as high-resolution grain-size indicators (Biskaborn et al. 2013; ESM). Fe/Mn ratios (Fig. 2b) are generally regarded as a proxy for redox conditions at the lake bottom (Boyle 2001) and thus reflect oxygen concentration at the bottom of Lake Karakul. We furthermore consider Br to be a complementary, high-resolution proxy for organic matter content, consistent with previous studies of marine (Mayer et al. 1981; Ziegler et al. 2008) and lake sediments (Kalugin et al. 2007;

Biskaborn et al. 2013; for details on XRF interpretation, see the ESM).

The PCA biplot displays relationships among the external lake proxies (Fig. 4a). Along the first axis, showing the external parameters, plotted proxies indicate coarser grain size (e.g. Zr/Rb as a detrital input and mean grain-size indicator) and imply fluvial input, with $\delta^{13}\text{C}_{\text{Carb}}$ and $\delta^{18}\text{O}_{\text{Carb}}$ reflecting the evaporation/freshwater input ratio on the negative end. Proxies reflecting fine grain size, such as EM1 and TiO_2 plot on the positive end of the axis. On the positive end of the second axis, plot EM4 (reflecting minerogenic matter moving through saltation on ice during periods of dry climate) and TiO_2 , which is assumed to enter the lake mainly as fine dust particles. EM3, which was identified as a fluvial indicator, and EM2, which might reflect glacial outwash or wet-deposited dust, plot on the negative end of the second axis. Although the $\text{PCA}_{\text{external}}$ axes scores show a more similar trend during the Holocene, they run opposite to one another during the late Pleistocene and LGM. We assume this is a consequence of glacial influence, which affects the transport mechanisms for the grain sizes represented by the end-members. EM1 and EM2 especially, are probably, in part, glacially derived sediments and reached the lake as “glacial milk” during the late Pleistocene.

The main data structure of the internal lake proxies is shown in Fig. 4b. TOC, TOC_{Br} and TOC/TN are indicators for bioproductivity and plot along the first $\text{PCA}_{\text{internal}}$ axis. The second $\text{PCA}_{\text{internal}}$ axis reflects lake-bottom ventilation and possibly lake-level changes, indicated by the strong correlation with the Fe/Mn ratio and TIC. Whereas Fe/Mn is often used as an indicator for redox conditions, carbonate precipitation as aragonite crystals from surface waters in a Mg^{2+} - and SO_4^{2-} -dominated, closed-basin lake, normally occurs during periods of sufficient runoff and relatively warm conditions, both facilitating the establishment of a more stratified water column with oxygen deficiency at the lake floor (Mischke et al. 2010). Thus, axis 2 of $\text{PCA}_{\text{internal}}$ possibly indicates lower lake levels with oxidizing conditions at the lake bottom clustering on the negative end, and higher lake levels on the positive end of the second PCA axis. The bioproductivity proxy cluster is uncoupled from the lake-level proxies, which supports our interpretation for the lake internal proxies.

Implications of the Lake Karakul sediment record

Pre-LGM to late glacial (28.6–13.3 cal ka BP)

The pre-LGM phase of the KK12-1 record (zone 1; Fig. 2a.2) is characterised by a high input of EM4 sediments, probably indicating strong local cold-season storms. Moderate values of EM1 and low values of EM2 probably reflect wet deposition of fine dust transported over long distances, but a generally low accumulation of coarser-grained dust and/or low glacial sediment input during this time. Moderate Zr/Rb and Sr/Rb ratios possibly result from the presence of feldspars and other detrital minerals (Kalugin et al. 2007; Kylander et al. 2011), whereas medium peaks coincide with EM4 peaks, suggesting an input of coarser-grained sediments. High $\delta^{18}\text{O}_{\text{Carb}}$ values could result from marked aridity and strong evaporation from the lake surface, which was apparently not sealed by long-lasting ice cover.

EM4 reaches high proportions between 22 and 20 cal ka BP, pointing towards dry and stormy winters. Relatively arid and cold conditions that prevailed during the LGM are consistent with the dominance of EM2 sediments in the core. Generally decreasing $\delta^{18}\text{O}_{\text{Carb}}$ values during the LGM presumably result from global cooling, which led to isotopically depleted precipitation in the Karakul region, and decreasing evaporation effects from the lake surface, as a consequence of prolonged periods of ice cover.

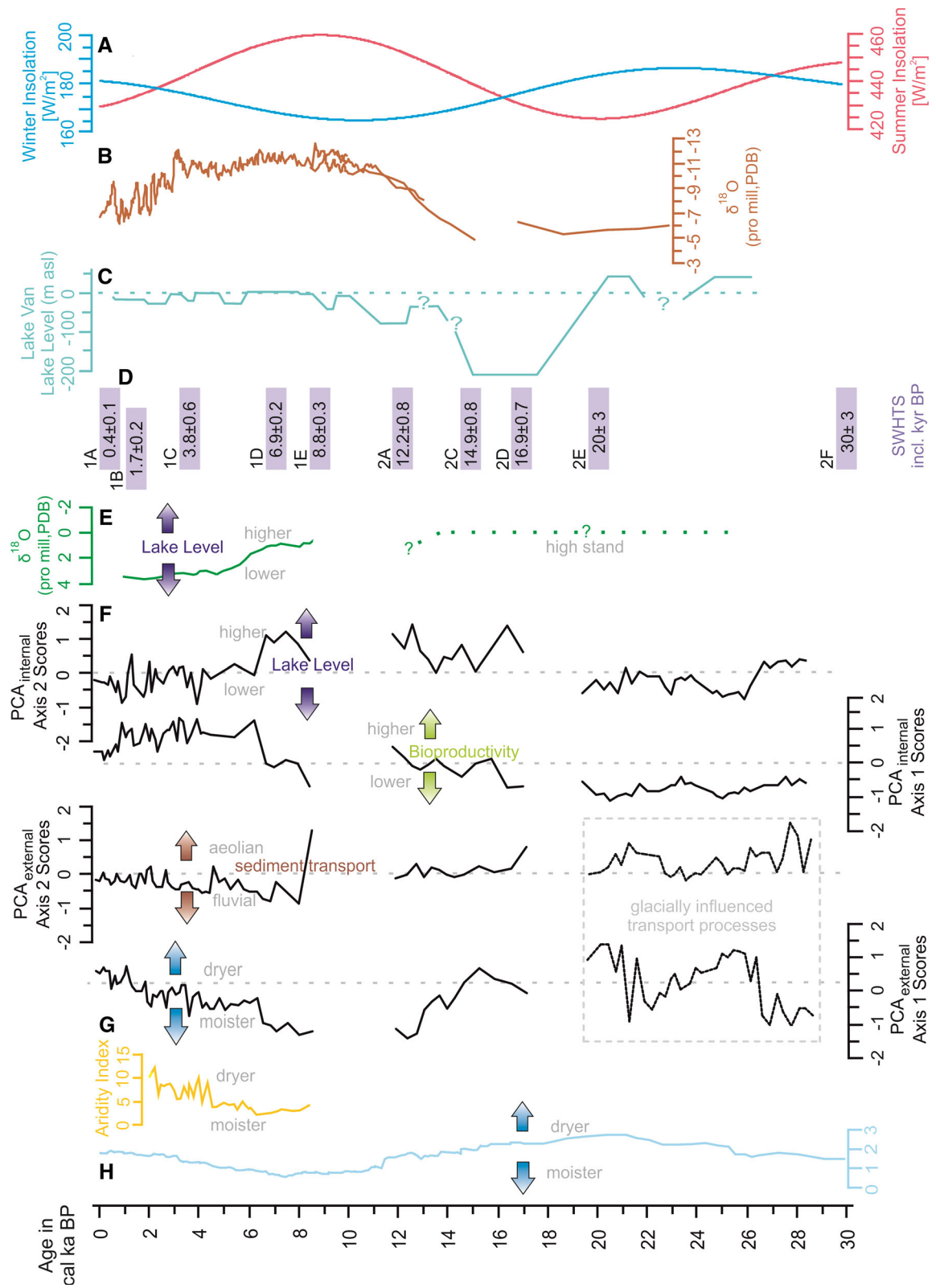
High values of EM1 during the late glacial could point towards persistent long-distance transport, presumably recording a Westerly influence and fine-dust accumulation with precipitation (Wu et al. 2006; Vandenberghe et al. 2006) or increased sediment-rich glacial meltwater (Liu et al. 2014; Wang et al. 2015). Increasing EM3 values suggest marked fluvial input to the lake, likely caused by increasing temperatures and glacial meltwater discharge, which might also be reflected by slightly increasing Zr/Rb and Sr/Rb values and increased mean grain size of detrital input (Biskaborn et al. 2013; ESM). Accordingly, high $\delta^{18}\text{O}_{\text{Carb}}$ values probably result from relatively warm temperatures, isotopically less depleted precipitation in the Lake Karakul region, and enhanced evaporation from the lake surface during a longer ice-free period.

Zech et al. (2005) claimed there were glacial advances around 27 ka BP in the southern Pamirs. Dortch et al. (2013), investigating glacial deposits in

the western Himalayan range using ^{10}Be surface exposure ages, proposed several glacial advances, termed semi-arid western Himalayan–Tibetan stages (SWHTS). One SWHTS, named 2F, occurred around 30 ± 3 ka BP (Fig. 5) and three other local glacial stages in the Himalayan–Tibetan mountains were dated between 17 and 14 ka BP. They were apparently synchronous with the Oldest Dryas and Heinrich event 1 of the Northern Hemisphere and were likely controlled by precipitation from the Westerlies. Owen and Dortch (2014) compare the SWHTS with Monsoonal Himalayan–Tibetan stages (MOHITS; Murari et al. 2014) and argued that at times SWHTS and MOHITS were concurrent and probably had similar moisture sources, whereas at other times only one of the stages is evident, implying differing climate controls. Komatsu and Tsukamoto (2015) recorded a late glacial glacier advance in the Karakul catchment at 15 ka BP and suggested that glaciers responded to enhanced moisture availability from the Westerlies. Their suggestion is in agreement with increased Westerlies precipitation (EM1), higher fluvial input or increased glacial meltwater discharge (EM3) to the lake, inferred from the KK12-1 core.

End of the late glacial and early to middle Holocene (13.3–6.6 cal ka BP)

Indicators that mainly reflect fine aeolian input to the lake, EM1 and 2, in combination with TiO_2 , display low values between the end of the late glacial and the early Holocene (zone 2; Fig. 2a.2), and high values of EM3 imply increased fluvial input. This could be a consequence of increased precipitation and surface runoff or glacier melt. No evidence, however, has yet been found, which suggests that glaciers came close to the lake during the early to middle Holocene. A maximum of EM4 and the residual EM at ca. 8.5 cal ka BP may indicate the occurrence of especially dry and stormy winters, analogous to the LGM, or more likely, the formation of a single event layer of aeolian sand. Maximum Sr/Rb and Zr/Rb ratios probably reflect increased grain-size associated with higher input of EM3 and EM4, and signal coarser detrital input. The $\delta^{18}\text{O}_{\text{Carb}}$ values are high at the end of the late glacial and during the early and middle Holocene, most likely reflecting rising global temperatures and the arrival of less depleted precipitation in Lake Karakul's catchment. The high $\delta^{18}\text{O}_{\text{Carb}}$ values



◀ **Fig. 5** Comparison of the Lake Karakul record with **a** summer and winter insolation at 40°N (Laskar et al. 2004); **b** Kesang cave (Cheng et al. 2012); **c** lake level changes of Lake Van (Çağatay et al. 2014); **d** semi-arid western Himalaya–Tibetan Stages (Dortch et al. 2013); **e** lake level changes from Lake Issyk-Kul (Ricketts et al. 2001; Romanovsky 2002); **f** PCA axis scores for lake internal and lake external parameters from Lake Karakul, Tajikistan, this study; **g** pollen-derived aridity Index from Lake Son Kul (Mathis et al. 2014); **h** mean effective moisture from monsoonal Central Asia (Herzschuh 2006)

could have been caused by increased evaporation that resulted from higher temperatures and shorter ice-cover periods. A marked change in moisture availability towards wetter conditions in the study region is reflected in this zone.

Global temperature rose strongly during the Bølling/Allerød and early Holocene until approximately 9.5 ka BP, and stayed high until about 5.5 ka BP (Marcott et al. 2013). Seong et al. (2009) inferred several glacial advances in the Muztag Ata and Kongur Shan Mountains during the early Holocene and argued for moisture transport from the middle latitude Westerlies, supported by the pollen-derived aridity index from Lake Son Kul (Fig. 5; Mathis et al. 2014).

6.6 cal ka BP until present

From 6.6 cal ka BP onward (zone 3; Fig. 2a.2) EM1 and EM2 show an increasing trend, reflecting enhanced influence of drier air masses. EM4 shows a more sporadic pattern towards the present day, which likely reflects reduced winter storms and the weakening influence of the Siberian High. EM3 displays slightly declining values that accelerated in the last 2 cal ka, also implying decreasing fluvial input, caused by either less moisture availability or a lower input of glacier-transported material, given the great distances of glaciers from the lake and coring location. Decreasing Sr/Rb and Zr/Rb ratios correspond to a decreasing mean grain size and a steady increase in TiO₂, emphasizing the increasing long-distance dust input. Declining δ¹⁸O_{Carb} values are probably recording the global cooling trend since the middle Holocene, with ¹⁸O-depleted incoming moisture and reduced evaporation (Taft et al. 2014).

Liu et al. (2014) investigated glacial activity in the westernmost Tibetan Plateau using multi-proxy analyses of glacio-lacustrine sediments from Lake

Karakuli (~150 km SE of Lake Karakul) and found a general correlation between local glacier advances and Holocene ice-rafting events in the northern Atlantic. Sediments from Lake Son Kul (~340 km NE of Lake Karakul) in the Tien Shan Mountains show a moderate drying trend, with negative water balance, and only a few decadal to centennial reversals between 8.2 and 2 cal ka BP (Huang et al. 2014; Lauterbach et al. 2014). Ricketts et al. (2001) infer a wet period preceding 6.9 cal ka BP for Lake Issyk-Kul (~480 km NE of Lake Karakul), suggesting increased moisture transport from the west or possible Asian Monsoon influence. This is in accordance with findings by Mathis et al. (2014) at Lake Son Kul, whose aridity index implies moister conditions from ca. 8.4 to 4.5 cal ka BP, and drier conditions thereafter (Fig. 5).

Linking lake internal development to climate change

Pre-LGM and LGM (28.6–19.2 cal ka BP)

Low PCA_{internal} axis 1 sample scores and low TOC suggest low bioproductivity and poor preservation of organic matter (Meyers and Lallier-Vergés 1999). The bioproductivity reaches a minimum during the LGM. Moderate TIC and PCA_{internal} axis 2 values during the pre-LGM show that inflow to the lake and resulting carbonate precipitation were still significant before the onset of the LGM. TIC and PCA_{internal} axis 2 values decreased rapidly towards the LGM. Thus, decreased inflow, reduced carbonate precipitation and low lake level prevailed during the LGM. Low Fe/Mn ratios, as a redox proxy, imply a well-mixed waterbody with sufficient dissolved oxygen at the lake bottom (Boyle 2001; Cohen 2003). This inference is consistent with the reconstructed cold and windy climate. Accordingly, climate is surmised to have been the main driver of the lake's internal conditions during the pre-LGM and LGM. Very low TOC values have also been recorded on the Tibetan Plateau, suggesting low bioproductivity and cold temperatures during the LGM (Zhang and Mischke 2009; An et al. 2012; Zhu et al. 2015). Although only few dates are available at Lake Issyk-Kul in Kyrgyzstan, situated NE of lake Karakul, lacustrine terrace sediments 33 m above current lake level indicate a period of lake-level highstands starting around 26 ka BP and lasting until the

late glacial (Fig. 5; literature in Russian quoted in Romanovsky (2002) and Ricketts et al. (2001)). Similar dates for high-stands were recorded for Lake Van in eastern Turkey (Fig. 5), west of our study region, at approximately 26 cal ka BP and the end of the LGM (Çağatay et al. 2014). Moderate to low lake levels were reconstructed for Lake Karakul during this period.

Late glacial and early to mid-Holocene (17.5 to ca. 6.9 cal ka BP)

A slight increase in bioproductivity is indicated by the continuously increasing $PCA_{internal}$ axis 1 and TOC values (Meyers and Lallier-Vergés 1999). TIC values rise rapidly and reach maximum values during the late glacial, indicating high runoff and enhanced carbonate precipitation. The Fe/Mn ratios show a marked increase during the late glacial and culminate during the onset of the Holocene, implying reducing conditions at the lake bottom (Cohen 2003). The $PCA_{internal}$ axis 2 scores are high during the late glacial and early to middle Holocene, probably reflecting a high lake level (zone 2; Fig. 2b). This inference is supported by the study of Komatsu and Tsukamoto (2015) who proposed a maximum lake level of 35 m above the modern stage during the late glacial and provide field evidence of glaciers reaching the lake at 15 ka BP. This coincides with several glacier advances (SWTHS 2D-2A) during the late glacial recorded by Dortch et al. (2013) (Fig. 5) and Seong et al. (2009), who investigated moraines in the Muztag Ata and Kongur Shan massifs 170 km SE of Lake Karakul, suggesting glacial advances around 17 and 13.7 ka BP. In contrast, lakes farther west of Lake Karakul, such as Lake Van, experienced a rapid drop in lake level after 21 cal ka BP (Landmann et al. 1996; Çağatay et al. 2014).

Early Holocene TOC values remained relatively low in contrast to rapidly increasing Fe/Mn ratios (zone 2; Fig. 2b). The high TIC values indicate that runoff to the lake was high. In consequence, a relatively unchanged bioproductivity and rapidly increasing lake level is inferred for the early Holocene, which led to the establishment of poorly oxygenated bottom waters in Lake Karakul. The inferred moderate bioproductivity in the lake possibly resulted from relatively low lake-water temperatures, in comparison to air temperatures, a consequence of enhanced input

of glacial meltwater. We thus suggest that climate was the main driver of the internal lake development.

Ricketts et al. (2001) examined trace elements and $\delta^{18}O$ values of ostracod shells from Lake Issyk-Kul and inferred high freshwater input to the lake from the beginning of their record at 8.7–8.3 cal ka BP. They speculated about a northward extension of the Asian Monsoon in the early Holocene as a result of the higher summer insolation. It remains unclear, however, whether or not the northward extension of the Asian Monsoon in the early Holocene existed and reached the study region. A relatively stable, high lake level with sufficient inflow prevailed at Lake Issyk-Kul until 6.9 cal ka BP, consistent with our findings for the early and middle Holocene.

6.6 cal ka BP until present

High TOC values and $PCA_{internal}$ axis 1 scores signal high bioproductivity during the last 6.6 cal ka BP (zone 3; Fig. 2b). Values for TOC/TN between 10 and 16 reflect a shift in organic matter origin from purely planktonic to more mixed sources: planktonic, macrophytes, macroalgae, and/or terrestrial. This shift was most likely caused by an increase in the amount of submerged macrophytes, of which abundant remains are recorded in the upper part of the core. Continuously decreasing Fe/Mn ratios point towards increasing ventilation, likely caused by decreasing lake level and better oxygenation of bottom waters. The inferred lower lake level after 6.6 cal ka BP likely resulted from a shift from moister to drier conditions, and from reduced meltwater inflow. The decreasing TIC values probably reflect decreasing inflow. Hence, internal lake development was mainly related to climate aridification during the last 6.6 cal ka.

A similar development is inferred at Lake Issyk-Kul, where the $\delta^{18}O$ values of ostracod shells suggest a major change in lake hydrology between 6.9 and 4.9 cal ka BP (Ricketts et al. 2001; Fig. 5), which led to a shift from an open-lake system to a mostly closed-lake system related to increasing aridity compared to the middle Holocene. Ricketts et al. (2001) suggested increased biological productivity at Lake Issyk-Kul during the second half of the Holocene, after the shift to a closed system, corresponding to our findings from Lake Karakul for the last 6.6 cal ka. Sedimentological studies from Lake Son Kul in the Tian Shan Mountains recorded a similar drying trend, interrupted by short

intervals of moister conditions (Huang et al. 2014; Lauterbach et al. 2014), while pollen-derived data indicate a shift from moister to drier conditions at 5.0–4.5 cal ka BP (Mathis et al. 2014; Fig. 5). A trend towards cooler conditions from about 3.5 to 1.9 cal ka BP was reported for Lake Karakul by Mischke et al. (2010) who investigated the last 4.2 ka BP at high resolution. Low TOC values and low Fe/Mn ratios in core KK12-1 support these interpretations, implying decreased bioproductivity and increased mixing and ventilation of the lake floor. After approximately 1.9 cal ka BP, a warmer phase led to increased meltwater supply (Mischke et al. 2010; Taft et al. 2014), reflected by increased Fe/Mn values in core KK12-1 until 0.6 ka BP. Similarly, a warm, but not moist period was observed elsewhere in Central Asia, such as at Lake Karakuli (Aichner et al. 2015), which could be indicative of the Medieval Warm Period (MWP). Afterwards, drier conditions prevailed, possibly reflecting the Little Ice Age, in accordance with the inferences of Mischke et al. (2010).

Conclusions

We identified three main climate phases over the last 29 ka, using multiple variables in a sediment core from Lake Karakul, Tajikistan. The Karakul region was influenced by relatively dry conditions and long-distant transport of aeolian sediments during the pre-LGM, LGM and late glacial. Moister conditions prevailed towards the end of the glacial and in the early and first half of the middle Holocene, until ca. 6.6 cal ka BP. During the second half of the middle Holocene, a drying trend set in, most likely caused by drier air masses transported by the Westerlies, and arid conditions in the Pamir Mountains prevailed during the late Holocene and lasted until today.

Reconstructed changes within the lake were mainly related to changes in the productivity and redox conditions at the lake bottom. Low lake level, coinciding with high ventilation and low productivity, prevailed during the pre-LGM and LGM at Lake Karakul, followed by a lake-level high-stand during the late glacial and early to middle Holocene (17.5 until ~6.6 cal ka BP). Productivity increased rapidly, with enhanced ventilation and declining lake levels from 6.6 cal ka BP onwards. Comparisons of lake internal signals from Lake Karakul with those from

other relatively deep lakes in the Westerlies region suggest that the sedimentation regime in Lake Karakul was driven largely by climate, which is not unexpected, as it is mainly fed by glacial meltwater.

Acknowledgements We thank Zafar Mahmoudov and Tim Jonas for help during fieldwork, Romy Zibulski for identification and discussions of the moss remains, and Matthias Röhl for support with core description. We furthermore thank Mark Brenner and two anonymous reviewers for their comments, which helped to improve this manuscript. We appreciate the financial support of the DFG (Grants Mi 730/15-1 and 15-2; and PhD scholarship for LH in the DFG Graduate School 1364).

Data Availability The datasets generated and analysed for this study are available at Pangaea, doi:10.1594/PANGAEA.876024.

References

- Abramowski U, Bergau A, Seebach D, Zech R, Glaser B, Sosin P, Kubik PW, Zech W (2006) Pleistocene glaciations of Central Asia: results from ^{10}Be surface exposure ages of erratic boulders from the Pamir (Tajikistan), and the Alay-Turkestan range (Kyrgyzstan). *Quat Sci Rev* 25:1080–1096. doi:10.1016/j.quascirev.2005.10.003
- Aichner B, Feakins SJ, Lee JE, Herzsuh U, Liu X (2015) High-resolution leaf wax carbon and hydrogen isotopic record of the late Holocene paleoclimate in arid Central Asia. *Clim Past* 11:619–633
- Aizen EM, Aizen VB, Melack JM, Nakamura T, Ohta T (2001) Precipitation and atmospheric circulation patterns at mid-latitudes of Asia. *Int J Climatol* 21:535–556. doi:10.1002/joc.626
- An Z, Colman SM, Zhou W, Li X, Brown ET, Jull AJT, Cai Y, Huang Y, Lu X, Chang H, Song Y, Sun Y, Xu H, Liu W, Jin Z, Liu X, Cheng P, Liu Y, Ai L, Li X, Liu X, Yan L, Shi Z, Wang X, Wu F, Qiang X, Dong J, Lu F, Xu X (2012) Interplay between the Westerlies and Asian monsoon recorded in Lake Qinghai sediments since 32 ka. *Sci Rep*. doi:10.1038/srep00619
- Biskaborn BK, Herzsuh U, Bolshiyarov DY, Schwamborn G, Diekmann B (2013) Thermokarst processes and depositional events in a tundra lake, Northeastern Siberia. *Permafrost Periglacial Process* 24:160–174. doi:10.1002/ppp.1769
- Blaauw M, Christen JA (2011) Flexible paleoclimate age-depth models using an autoregressive gamma process. *Bayesian Anal* 6:457–474. doi:10.1214/ba/1339616472
- Böhner J (2006) General climatic controls and topoclimatic variations in Central and High Asia. *Boreas* 35:279–295. doi:10.1111/j.1502-3885.2006.tb01158.x
- Boulton GS (1978) Boulder shapes and grain-size distributions of debris as indicators of transport paths through a glacier and till genesis. *Sedimentology* 25:773–799. doi:10.1111/j.1365-3091.1978.tb00329.x
- Boyle JF (2001) Inorganic geochemical methods in palaeolimnology. In: Last WM, Smol JP (eds) *Tracking*

- environmental change using lake sediments. Kluwer Academic Publishers, Dordrecht, pp 83–141
- Çağatay MN, Öğretmen N, Damcı E, Stockhecke M, Sancar Ü, Eriş KK, Özeren S (2014) Lake level and climate records of the last 90 ka from the Northern Basin of Lake Van, eastern Turkey. *Quat Sci Rev* 104:97–116. doi:[10.1016/j.quascirev.2014.09.027](https://doi.org/10.1016/j.quascirev.2014.09.027)
- Chen F-H, Chen J-H, Holmes J, Boomer I, Austin P, Gates JB, Wang N-L, Brooks SJ, Zhang J-W (2010) Moisture changes over the last millennium in arid Central Asia: a review, synthesis and comparison with monsoon region. *Quat Sci Rev* 29:1055–1068. doi:[10.1016/j.quascirev.2010.01.005](https://doi.org/10.1016/j.quascirev.2010.01.005)
- Cheng H, Zhang PZ, Spötl C, Edwards RL, Cai YJ, Zhang DZ, Sang WC, Tan M, An ZS (2012) The climatic cyclicality in semiarid-arid central Asia over the past 500,000 years. *Geophys Res Lett* 39:L01705. doi:[10.1029/2011GL015020](https://doi.org/10.1029/2011GL015020)
- Cohen AS (2003) *Paleolimnology: the history and evolution of lake systems*. Oxford University Press, USA
- Core Team R (2012) R: a language and environment for statistical computing. R Foundation for Statistical Computing, Vienna
- Dietze M, Dietze E (2013) EMMAgeo: end-member modelling algorithm and supporting functions for grain-size analysis, R package version 0.9.0
- Dietze E, Hartmann K, Diekmann B, IJmker J, Lehmkuhl F, Opitz S, Stauch G, Wünnemann B, Borchers A (2012) An end-member algorithm for deciphering modern detrital processes from lake sediments of Lake Donggi Cona, NE Tibetan Plateau China. *Sediment Geol*. doi:[10.1016/j.sedgeo.2011.09.014](https://doi.org/10.1016/j.sedgeo.2011.09.014)
- Dortch JM, Owen LA, Caffee MW (2013) Timing and climatic drivers for glaciation across semi-arid western Himalayan–Tibetan orogen. *Quat Sci Rev* 78:188–208. doi:[10.1016/j.quascirev.2013.07.025](https://doi.org/10.1016/j.quascirev.2013.07.025)
- Ergashev AE (1979) The origin and typology of the Central Asian lakes and their algal flora. *Int Rev Gesamten Hydrobiol* 64:629–642
- Fey M, Korr C, Maidana NI, Carrevedo ML, Corbella H, Dietrich S, Haberzettl T, Kuhn G, Lücke A, Mayr C, Ohlendorf C, Paez MM, Quintana FA, Schäbitz F, Zolitschka B (2009) Palaeoenvironmental changes during the last 1600 years inferred from the sediment record of a cirque lake in southern Patagonia (Laguna Las Vizcachas, Argentina). *Long-Term Multi-Proxy Clim Reconstr Dyn S Am LOTRED-SA State Art Perspect* 281:363–375. doi:[10.1016/j.palaeo.2009.01.012](https://doi.org/10.1016/j.palaeo.2009.01.012)
- Fuchs MC, Gloaguen R, Merchel S, Pohl E, Sulaymonova VA, Andermann C, Rugel G (2015) Millennial erosion rates across the Pamir based on ¹⁰Be concentrations in fluvial sediments: dominance of topographic over climatic factors. *Earth Surf Dyn Discuss* 3:83–128
- Grimm EC (1987) CONISS: a FORTRAN 77 program for stratigraphically constrained cluster analysis by the method of incremental sum of squares. *Comput Geosci* 13:13–35
- Hammer UT (1986) *Saline lake ecosystems of the world*. Springer, Berlin
- Herzschuh U (2006) Palaeo-moisture evolution in monsoonal Central Asia during the last 50,000 years. *Quat Sci Rev* 25:163–178. doi:[10.1016/j.quascirev.2005.02.006](https://doi.org/10.1016/j.quascirev.2005.02.006)
- Huang X, Oberhänsli H, von Suchodoletz H, Prasad S, Sorrel P, Plessen B, Mathis M, Usabaliev R (2014) Hydrological changes in western Central Asia (Kyrgyzstan) during the Holocene as inferred from a palaeolimnological study in lake Son Kul. *Quat Sci Rev* 103:134–152. doi:[10.1016/j.quascirev.2014.09.012](https://doi.org/10.1016/j.quascirev.2014.09.012)
- Kalugin I, Daryin A, Smolyaninova L, Andreev A, Diekmann B, Khlystov O (2007) 800-yr-long records of annual air temperature and precipitation over southern Siberia inferred from Teletskoye Lake sediments. *Quat Res* 67:400–410. doi:[10.1016/j.yqres.2007.01.007](https://doi.org/10.1016/j.yqres.2007.01.007)
- Komatsu T, Tsukamoto S (2015) Late Glacial lake-level changes in the Lake Karakul basin (a closed glacierized-basin), eastern Pamirs, Tajikistan. *Quat Res* 83:137–149. doi:[10.1016/j.yqres.2014.09.001](https://doi.org/10.1016/j.yqres.2014.09.001)
- Kylander ME, Ampel L, Wohlfarth B, Veres D (2011) High-resolution X-ray fluorescence core scanning analysis of Les Echets (France) sedimentary sequence: new insights from chemical proxies. *J Quat Sci* 26:109–117. doi:[10.1002/jqs.1438](https://doi.org/10.1002/jqs.1438)
- Landmann G, Reimer A, Lemcke G, Kempe S (1996) Dating Late Glacial abrupt climate changes in the 14,570 yr long continuous varve record of Lake Van, Turkey. *Palaeogeogr Palaeoclimatol Palaeoecol* 122:107–118. doi:[10.1016/0031-0182\(95\)00101-8](https://doi.org/10.1016/0031-0182(95)00101-8)
- Laskar J, Robutel P, Joutel F, Gastineau M, Correia ACM, Levrard B (2004) A long-term numerical solution for the insolation quantities of the Earth. *Astron Astrophys* 428:261–285. doi:[10.1051/0004-6361:20041335](https://doi.org/10.1051/0004-6361:20041335)
- Lauterbach S, Witt R, Plessen B, Dulski P, Prasad S, Mingram J, Gleixner G, Hettler-Riedel S, Stebich M, Schnetger B, Schwalb A, Schwarz A (2014) Climatic imprint of the mid-latitude Westerlies in the Central Tian Shan of Kyrgyzstan and teleconnections to North Atlantic climate variability during the last 6000 years. *Holocene* 24:970–984. doi:[10.1177/0959683614534741](https://doi.org/10.1177/0959683614534741)
- Liu X, Herzschuh U, Wang Y, Kuhn G, Yu Z (2014) Glacier fluctuations of Muztagh Ata and temperature changes during the late Holocene in westernmost Tibetan Plateau, based on glaciolacustrine sediment records. *Geophys Res Lett* 41:6265–6273. doi:[10.1002/2014GL060444](https://doi.org/10.1002/2014GL060444)
- Marcott SA, Shakun JD, Clark PU, Mix AC (2013) A reconstruction of regional and global temperature for the past 11,300 years. *Science* 339:1198–1201. doi:[10.1126/science.1228026](https://doi.org/10.1126/science.1228026)
- Mathis M, Sorrel P, Klotz S, Huang X, Oberhänsli H (2014) Regional vegetation patterns at lake Son Kul reveal Holocene climatic variability in central Tien Shan (Kyrgyzstan, Central Asia). *Quat Sci Rev* 89:169–185. doi:[10.1016/j.quascirev.2014.01.023](https://doi.org/10.1016/j.quascirev.2014.01.023)
- Mayer LM, Macko SA, Mook WH, Murray S (1981) The distribution of bromine in coastal sediments and its use as a source indicator for organic matter. *Org Geochem* 3:37–42. doi:[10.1016/0146-6380\(81\)90011-5](https://doi.org/10.1016/0146-6380(81)90011-5)
- Meyers PA, Lallier-Vergés E (1999) Lacustrine sedimentary organic matter records of Late Quaternary paleoclimates. *J Paleolimnol* 21:345–372. doi:[10.1023/A:1008073732192](https://doi.org/10.1023/A:1008073732192)
- Mischke S, Rajabov I, Mustaeva N, Zhang C, Herzschuh U, Boomer I, Brown ET, Andersen N, Myrbo A, Ito E, Schudack ME (2010) Modern hydrology and late Holocene history of Lake Karakul, eastern Pamirs (Tajikistan): a

- reconnaissance study. *Palaeogeogr Palaeoclimatol Palaeoecol* 289:10–24. doi:[10.1016/j.palaeo.2010.02.004](https://doi.org/10.1016/j.palaeo.2010.02.004)
- Mischke S, Weynell M, Zhang C, Wiechert U (2013) Spatial variability of ^{14}C reservoir effects in Tibetan Plateau lakes. *Quat Int* 313–314:147–155. doi:[10.1016/j.quaint.2013.01.030](https://doi.org/10.1016/j.quaint.2013.01.030)
- Morrill C, Overpeck JT, Cole JE, Liu K, Shen C, Tang L (2006) Holocene variations in the Asian monsoon inferred from the geochemistry of lake sediments in central Tibet. *Quat Res* 65:232–243. doi:[10.1016/j.yqres.2005.02.014](https://doi.org/10.1016/j.yqres.2005.02.014)
- Murari MK, Owen LA, Dortch JM, Caffee MW, Dietsch C, Fuchs M, Haneberg WC, Sharma MC, Townsend-Small A (2014) Timing and climatic drivers for glaciation across monsoon-influenced regions of the Himalayan–Tibetan orogen. *Quat Sci Rev* 88:159–182. doi:[10.1016/j.quascirev.2014.01.013](https://doi.org/10.1016/j.quascirev.2014.01.013)
- Ni A, Nurtayev B, Petrov M, Tikhanovskaya A, Tomashevskaya I (2004) The share of a glacial feeding in water balance of Aral Sea and Karakul Lake. *J Mar Syst* 47:143–146. doi:[10.1016/j.jmarsys.2003.12.017](https://doi.org/10.1016/j.jmarsys.2003.12.017)
- Owen LA, Dortch JM (2014) Nature and timing of Quaternary glaciation in the Himalayan–Tibetan orogen. *Quat Sci Rev* 88:14–54. doi:[10.1016/j.quascirev.2013.11.016](https://doi.org/10.1016/j.quascirev.2013.11.016)
- Pachauri RK, Allen MR, Barros VR, Broome J, Cramer W, Christ R, Church JA, Clarke L, Dahe Q, Dasgupta P, Dubash NK, Edenhofer O, Elgizouli I, Field CB, Forster P, Friedlingstein P, Fuglestedt J, Gomez-Echeverri L, Hallegatte S, Hegerl G, Howden M, Jiang K, Jimenez Cisneros B, Kattsov V, Lee H, Mach KJ, Marotzke J, Mastrandrea MD, Meyer L, Minx J, Mulugetta Y, O'Brien K, Oppenheimer M, Pereira JJ, Pichs-Madruga R, Plattner G-K, Pörtner H-O, Power SB, Preston B, Ravindranath NH, Reisinger A, Riahi K, Rusticucci M, Scholes R, Seyboth K, Sokona Y, Stavins R, Stocker TF, Tschakert P, van Vuuren D, van Ypersele J-P (2014) Climate change 2014: synthesis report. Contribution of Working Groups I, II and III to the fifth assessment report of the Intergovernmental Panel on Climate Change. IPCC, Geneva
- Pielke RA, Avissar R, Raupach M, Dolman AJ, Zeng X, Denning AS et al (1998) Interactions between the atmosphere and terrestrial ecosystems: influence on weather and climate. *Glob Change Biol* 4:461–475
- Ramaswamy C (1962) Breaks in the Indian summer monsoon as a phenomenon of interaction between the easterly and the sub-tropical westerly jet streams. *Tellus* 14:337–349. doi:[10.1111/j.2153-3490.1962.tb01346.x](https://doi.org/10.1111/j.2153-3490.1962.tb01346.x)
- Reimer PJ, Brown TA, Reimer RW (2004) Discussion: reporting and calibration of post-bomb ^{14}C data. *Radiocarbon* 46:1299–1304
- Ricketts RD, Johnson TC, Brown ET, Rasmussen KA, Romanovsky VV (2001) The Holocene paleolimnology of Lake Issyk-Kul, Kyrgyzstan: trace element and stable isotope composition of ostracodes. *Palaeogeogr Palaeoclimatol Palaeoecol* 176:207–227. doi:[10.1016/S0031-0182\(01\)00339-X](https://doi.org/10.1016/S0031-0182(01)00339-X)
- Romanovsky VV (2002) Water level variations and water balance of Lake Issyk-Kul. In: Klerkx J, Imanackunov B (eds) *Lake Issyk-Kul: its natural environment*. Springer, Netherlands, pp 45–57
- Seong YB, Owen LA, Yi C, Finkel RC (2009) Quaternary glaciation of Muztag Ata and Kongur Shan: evidence for glacier response to rapid climate changes throughout the Late Glacial and Holocene in westernmost Tibet. *Geol Soc Am Bull* 121:348–365. doi:[10.1130/B26339.1](https://doi.org/10.1130/B26339.1)
- Shen J, Liu X, Wang S, Matsumoto Ryo (2005) Palaeoclimatic changes in the Qinghai Lake area during the last 18,000 years. *Quat Int* 136:131–140. doi:[10.1016/j.quaint.2004.11.014](https://doi.org/10.1016/j.quaint.2004.11.014)
- Strecker MR, Frisch W, Hamburger MW, Ratschbacher L, Semiletkin S, Zamoruyev A, Sturchio N (1995) Quaternary deformation in the Eastern Pamirs, Tadzhikistan and Kyrgyzstan. *Tectonics* 14:1061–1079. doi:[10.1029/95TC00927](https://doi.org/10.1029/95TC00927)
- Sun D, Bloemendal J, Rea DK, Vandenberghe J, Jiang F, An Z, Su R (2002) Grain-size distribution function of polymodal sediments in hydraulic and aeolian environments, and numerical partitioning of the sedimentary components. *Sediment Geol* 152:263–277. doi:[10.1016/S0037-0738\(02\)00082-9](https://doi.org/10.1016/S0037-0738(02)00082-9)
- Taft L, Mischke S, Wiechert U, Leipe C, Rajabov I, Riedel F (2014) Sclerochronological oxygen and carbon isotope ratios in *Radix* (Gastropoda) shells indicate changes of glacial meltwater flux and temperature since 4,200 cal yr BP at Lake Karakul, eastern Pamirs (Tajikistan). *J Paleolimnol* 52:27–41. doi:[10.1007/s10933-014-9776-4](https://doi.org/10.1007/s10933-014-9776-4)
- Talbot MR (1990) A review of the palaeohydrological interpretation of carbon and oxygen isotopic ratios in primary lacustrine carbonates. *Chem Geol Isot Geosci Sect* 80:261–279. doi:[10.1016/0168-9622\(90\)90009-2](https://doi.org/10.1016/0168-9622(90)90009-2)
- Ter Braak CJF, Šmilauer P (2012) Canoco reference manual and user's guide: software for ordination, version 5.0. Microcomputer Power, Ithaca
- Tsoar H, Pye K (1987) Dust transport and the question of desert loess formation. *Sedimentology* 34:139–153. doi:[10.1111/j.1365-3091.1987.tb00566.x](https://doi.org/10.1111/j.1365-3091.1987.tb00566.x)
- Van Campo E, Gasse F (1993) Pollen- and diatom-inferred climatic and hydrological changes in Sumxi Co Basin (Western Tibet) since 13,000 yr B.P. *Quat Res* 39:300–313. doi:[10.1006/qres.1993.1037](https://doi.org/10.1006/qres.1993.1037)
- Vandenberghe J (2013) Grain size of fine-grained windblown sediment: a powerful proxy for process identification. *Earth-Sci Rev* 121:18–30
- Vandenberghe J, Renssen H, van Huissteden K, Nugteren G, Konert M, Lu H, Dodonov A, Buyllaert J-P (2006) Penetration of Atlantic westerly winds into Central and East Asia. *Quat Sci Rev* 25:2380–2389. doi:[10.1016/j.quascirev.2006.02.017](https://doi.org/10.1016/j.quascirev.2006.02.017)
- Walling DE, Moorehead PW (1989) The particle size characteristics of fluvial suspended sediment: an overview. *Hydrobiologia* 176–177:125–149. doi:[10.1007/BF00026549](https://doi.org/10.1007/BF00026549)
- Wang R, Zhang Y, Wünnemann B, Biskaborn BK, Yin H, Xia F, Zhou L, Diekmann B (2015) Linkages between Quaternary climate change and sedimentary processes in Hala Lake, northern Tibetan Plateau, China. *J Asian Earth Sci* 107:140–150. doi:[10.1016/j.jseas.2015.04.008](https://doi.org/10.1016/j.jseas.2015.04.008)
- Weltje GJ (1997) End-member modeling of compositional data: numerical-statistical algorithms for solving the explicit mixing problem. *Math Geol* 29:503–549. doi:[10.1007/BF02775085](https://doi.org/10.1007/BF02775085)
- Weltje GJ, Tjallingii R (2008) Calibration of XRF core scanners for quantitative geochemical logging of sediment cores:

- theory and application. *Earth Planet Sci Lett* 274:423–438. doi:[10.1016/j.epsl.2008.07.054](https://doi.org/10.1016/j.epsl.2008.07.054)
- Williamson CE, Dodds W, Kratz TK, Palmer MA (2008) Lakes and streams as sentinels of environmental change in terrestrial and atmospheric processes. *Front Ecol Environ* 6:247–254. doi:[10.1890/070140](https://doi.org/10.1890/070140)
- Wu G, Yao T, Xu B, Li Z, Tian L, Duan K, Wen L (2006) Grain size record of microparticles in the Muztagata ice core. *Sci China Ser D* 49:10–17. doi:[10.1007/s11430-004-5093-5](https://doi.org/10.1007/s11430-004-5093-5)
- Zech R, Abramowski U, Glaser B, Sosin P, Kubik PW, Zech W (2005) Late Quaternary glacial and climate history of the Pamir Mountains derived from cosmogenic ^{10}Be exposure ages. *Quat Res* 64:212–220. doi:[10.1016/j.yqres.2005.06.002](https://doi.org/10.1016/j.yqres.2005.06.002)
- Zhang C, Mischke S (2009) A Lateglacial and Holocene lake record from the Nianbaoyeze Mountains and inferences of lake, glacier and climate evolution on the eastern Tibetan Plateau. *Quat Sci Rev* 28:1970–1983. doi:[10.1016/j.quascirev.2009.03.007](https://doi.org/10.1016/j.quascirev.2009.03.007)
- Zhao Y, Yu Z, Chen F, Zhang J, Yang B (2009) Vegetation response to Holocene climate change in monsoon-influenced region of China. *Earth-Sci Rev* 97:242–256. doi:[10.1016/j.earscirev.2009.10.007](https://doi.org/10.1016/j.earscirev.2009.10.007)
- Zhu L, Lü X, Wang J, Peng P, Kasper T, Daut G, Haberzettl T, Frenzel P, Li Q, Yang R, Schwalb A, Mäusbacher R (2015) Climate change on the Tibetan Plateau in response to shifting atmospheric circulation since the LGM. *Sci Rep* 5:13318. doi:[10.1038/srep13318](https://doi.org/10.1038/srep13318)
- Ziegler M, Jilbert T, de Lange GJ, Lourens LJ, Reichert G-J (2008) Bromine counts from XRF scanning as an estimate of the marine organic carbon content of sediment cores. *Geochem Geophys Geosystems*. doi:[10.1029/2007GC001932](https://doi.org/10.1029/2007GC001932)